INTERNATIONAL JOURNAL FOR NUMERICAL AND ANALYTICAL METHODS IN GEOMECHANICS, VOL. 21, 789–816 (1997)

A NOVEL FINITE ELEMENT DOUBLE POROSITY MODEL FOR MULTIPHASE FLOW THROUGH DEFORMABLE FRACTURED POROUS MEDIA

ROLAND W. LEWIS AND HAMID R. GHAFOURI

Civil Eng. Dept., University of Wales, Swansea-SA2 8PP U.K.

SUMMARY

Based on the theory of double-porosity, a novel mathematical model for multiphase fluid flow in a deforming fractured reservoir is developed. The present formulation, consisting of both the equilibrium and continuity equations, accounts for the significant influence of coupling between fluid flow and solid deformation, usually ignored in the reservoir simulation literature. A Galerkin-based finite element method is applied to discretize the governing equations both in the space and time domain. Throughout the derived set of equations the solid displacements as well as the fluid pressure values are considered as the primary unknowns and may be used to determine other reservoir parameters such as stresses, saturations, etc. The final set of equations represents a highly non-linear system as the elements of the coefficient matrices are updated during each iteration in terms of the independent variables. The model is employed to solve a field scale example where the results are compared to those of ten other uncoupled models. The results illustrate a significantly different behaviour for the case of a reservoir where the impact of coupling is also considered.

Int. J. Numer. Anal. Meth. Geomech., Vol. 21, 789–816 (1997)
(No. of Figures: 13 No. of Tables: 4 No. of Refs: 34)

Key words: Fractured reservoir; coupled model; finite elements

1. INTRODUCTION

Mathematical models with varying degrees of sophistication have been developed in the past to simulate flow through fractured porous media.[1–21] The initial models were generally very simple and were mainly based on the single porosity or continuum concept. In these models, a fractured system was grossly treated as an equivalent anisotropic continuum. A major departure from the single porosity approach was made by Barenblatt *et al.*[22] and later by Warren and Root.[23] They modelled a non-deformable highly fractured porous media as an entity having two porosities; one representing a fracture network and the other a continuum porous block. The fracture network was characterized by having very high permeabilty values and a very low storage while the porous blocks were characterized by low permeability and high storage. Kazemi *et al.*[24] extended Warren and Root's model to a more complex situation in two-dimensions. Later they also developed a three-dimensional, multi-well, model for simulating the two-phase flow of water and oil for a fractured reservoir.[25] Thomas *et al.*[26] proposed a three-dimensional, three-phase model

* Correspondence to R. W. Lewis, Civil Eng. Dept., University of Wales, Swansea SAZ 8PP, U.K.

CCC 0363–0961/97/110789–28$17.50

Received 24 November 1996
Revised 13 March 1997

for simulating the flow of water, oil and gas in a naturally fractured reservoir. In this model, primary flow in the reservoir occurs within the fractures with local exchange of fluids between the fractured system and the matrix blocks. All previous models developed for fractured reservoirs treated the reservoir either as a rigid body or, if not, the deformability effects were taken into account in an uncoupled manner, i.e. the interactive effect of the soil deformation and fluid flow were usually ignored, thus only the flow equations were required. The next natural step was to develop models that could account for deformability effects. Aifantis[27–29] presented a model coupling the soil deformation and single-phase fluid flow through a fractured porous media. More recently, Khalili[30] and Ghafouri *et al.*[31] employed the well-stabilised finite element method to develop a new double-porosity model for single-phase flow through a deformable fractured porous media. The studies identified the strong coupling between fluid flow and solid deformation.

The main objective of the present study is to introduce a rather realistic mathematical model for the case of multi-phase flow through a deformable fractured reservoir. The double-porosity model presented here has the same basic assumptions as Reference[31] where a strong coupling is assumed between the fluid flow and soil deformation. The governing equations, consisting of the equilibrium and continuity equations, are solved numerically by a standard Galerkin-based finite element method.

2. DESCRIPTION OF THE MODEL

The basic mechanism of fluid flow in a fractured porous media may be explained as follows: The applied external loads and/or well production both create a pressure gradient between the fluid within the matrix pores and the fluid in the adjacent fractures. The fluid within the matrix is squeezed out into the fissured continuum due to this gradient. Subsequently, flow towards the producing well takes place through the fissured network. In the present model, the fractured porous media is divided into two overlapping but distinct continua, the first represents flow and deformation in the porous matrix while the second represents flow in the fissures, Figure 1. These two sub-domains have the following characteristics:

1. The fluid flow within each sub-domain is independent of the flow in the other sub-domain and any coupling between the fluid flow in the porous matrix and the fissured network is controlled only via a *leakage* term, i.e. the fluid expelled from the matrix which enters the fissures and *vice versa*. Hence, fluid pressure, saturation, porosity, permeability and the other properties of both the soil and the fluids within the two sub-domains are considered separately.
2. Within the first continuum the fluid flow is assumed to be coupled with the matrix deformation. This coupling is controlled via the rate of change of volumetric strain $\partial \varepsilon_{v1}/\partial t$.
3. It is assumed that the deformation of the first sub-domain is due only to the total volumetric strain of the porous matrix and any change of volume of the solid particles is ignored.
4. Two different porosity values should be defined for the porous matrix and fissured region respectively, hence, the term *double porosity model*, as follows:

$$\varphi_1 = \frac{V_1}{V} \tag{1}$$

$$\varphi_2 = \frac{V_2}{V} \tag{2}$$

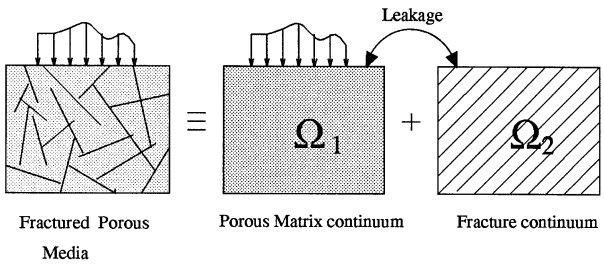

Figure 1. Schematic representation of double porosity model

where φ_1 and φ_2 are the porosity values of the porous matrix and fissured network, respectively, V_1 and V_2 are the pore and fissured volume in a representative elementary volume (REV) and V is the total volume.

5. We limit ourselves to the case of porous fractured reservoirs, where the volume of the fractures is normally a small fraction of the total void space. Therefore, it is assumed that both boundary and body forces are carried by the porous matrix sub-domain only and the contribution of the fracture continuum is ignored, see References 32 and 33.
6. Also, for the same reason, it is assumed that the compressibility of the fractured network does not alter the compressibility of the whole porous media dramatically and may be ignored, see References 32 and 33.
7. For the sake of simplicity we also limit ourselves to elastic behaviour with small deformations. However, other constitutive laws for the rock behaviour may also be utilized in a similar manner.
8. Fracture permeability is determined based on the geometry of the fracture and particularly on the dimensions of the aperture. If the fracture compressibility is neglected then the aperture, and consequently, the fracture absolute permeability, do not vary.
9. Imbibition and depletion of fluid is via the fissured network sub-domain only.
10. The two sub-domains are assumed to be fully saturated.

3. PRELIMINARY CALCULATIONS

As we shall see later, the main objective in these simulations is to determine the displacement and the fluid pressure within any given point of the domain. Any other information, such as capillary pressure, saturation, recovery, etc., then may be obtained in terms of these primary unknowns. Therefore, all other existing parameters must be converted to their appropriate forms before we can adequately formulate the equations to be used in a simulator. Accordingly, the next three sections are devoted to these preliminary calculations.

3.1. Capillary pressure relationships

A capillary pressure-saturation curve is used which is an approximation of both the drainage and the imbibition curves, Figure 2. Although it is possible to formulate a model that accounts for hysteresis resulting from the change of direction of flow, in most situations the directions of flow can be predicted and only one set of capillary pressure curves is required.

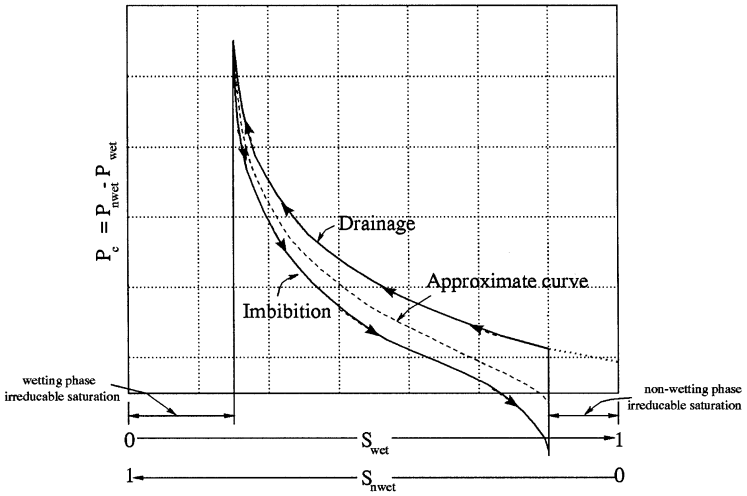

Figure 2. Capillary hysteresis characteristics

In a saturated oil reservoir, the fluid pressure values at any point are related by their capillary pressure relationships. In general, capillary pressure is defined as the difference between the non-wetting and the wetting phase pressure, i.e.,

$$P_c = P_{nwet} - P_{wet} \tag{3}$$

Therefore, for water-wet oil reservoirs, the following expressions are used:

For oil–water system,

$$P_{cw} = P_o - P_w \tag{4}$$

For oil–gas system,

$$P_{cg} = P_g - P_o \tag{5}$$

where P_{cw} is the capillary pressure for oil–water system (N/m^2), P_{cg} is the capillary pressure for oil–gas system (N/m^2) and, $P_{o,w,g}$ the oil, water and gas-phase pressure, respectively (N/m^2) or in differential form:

$$\frac{\partial P_{cw}}{\partial t} = \frac{\partial P_o}{\partial t} - \frac{\partial P_w}{\partial t} \tag{6}$$

$$\frac{\partial P_{cg}}{\partial t} = \frac{\partial P_g}{\partial t} - \frac{\partial P_o}{\partial t} \tag{7}$$

The chain rule may be applied to equations (6) and (7) which then result in

$$\frac{\partial S_w}{\partial t} = S'_w \left(\frac{\partial P_o}{\partial t} - \frac{\partial P_w}{\partial t} \right) \tag{8}$$

$$\frac{\partial S_g}{\partial t} = S'_g \left(\frac{\partial P_g}{\partial t} - \frac{\partial P_o}{\partial t} \right) \tag{9}$$

where $S_{o,w,g}$ is fluid saturation for oil, water, and gas phase, respectively, and

$$S'_w = \partial S_w/\partial P_{cw} \text{ is the slope of the plot } S_w \text{ vs. } P_{cw}$$

$$S'_g = \partial S_g/\partial P_{cg} \text{ is the slope of the plot } S_g \text{ vs. } P_{cg}.$$

It is also assumed that the pore volume is completely filled by a combination of the fluids present. Therefore, the sum of the fluid phase saturations must equal unity, i.e.,

$$S_o + S_g + S_w = 1 \tag{10}$$

This may also be written in a differential form a follows:

$$\frac{dS_o}{dt} = -\frac{dS_w}{dt} - \frac{dS_g}{dt} \tag{11}$$

Invoking the chain rule to equation (11) leads to the following:

$$\frac{\partial S_o}{\partial t} = -\frac{\partial S_w}{\partial P_{cw}}\frac{\partial P_{cw}}{\partial t} - \frac{\partial S_g}{\partial P_{cg}}\frac{\partial P_{cg}}{\partial t} \tag{12}$$

Incorporating equations (6) and (7) into equation (12), then this may be rearranged as follows

$$\frac{\partial S_o}{\partial t} = S'_w\frac{\partial P_w}{\partial t} + (S'_g - S'_w)\frac{\partial P_o}{\partial t} - S'_g\frac{\partial P_g}{\partial t} \tag{13}$$

Equations (8), (9) and (13) will be used in deriving $d\bar{P}/dt$ for determining the average pore pressure in a three-phase flow problem.

The capillarity effect has little or no influence in a fractured network. However, a small 'dummy' P_c–S_i curve, the best choice being a linear form, may be used for the fractured network. Fortunately, the value of dP_c/dS_i is small enough so that it does not affect the answers.

3.2. *Approximation of the average pore pressure*

The effective average pore pressure is calculated from

$$\bar{P} = S_oP_o + S_wP_w + S_gP_g \tag{14}$$

On differentiating equation (14) w.r.t. time we obtain;

$$\frac{\partial \bar{P}}{\partial t} = S_o\frac{\partial P_o}{\partial t} + P_o\frac{\partial S_o}{\partial t} + S_w\frac{\partial P_w}{\partial t} + P_w\frac{\partial S_w}{\partial t} + S_g\frac{\partial P_g}{\partial t} + P_g\frac{\partial S_g}{\partial t} \tag{15}$$

On incorporating equations (8), (9) and (13) into equation (15) and then simplifying, the following equation is obtained for the average pore pressure in a three-phase flow regime;

$$\frac{\partial \bar{P}}{dt} = S''_o\frac{\partial P_o}{\partial t} + S''_w\frac{\partial P_w}{\partial t} + S''_g\frac{\partial P_g}{\partial t} \tag{16}$$

where

$$S''_o = S_o - P_{cg}S'_g - P_{cw}S'_w \tag{17}$$

$$S''_w = S_w - P_{cw}S'_w \tag{18}$$

$$S''_g = S_g - P_{cg}S'_g \tag{19}$$

4. DEVELOPMENT OF THE EQUILIBRIUM EQUATION

In order to describe the solid-phase behaviour, the equation of equilibrium which takes into account the stress–strain relationship, must be considered. The equilibrium equation, relating the total stress σ_1 to the body force $\mathbf{b}$ and the boundary traction $\hat{\mathbf{t}}$ specified at the boundary Γ of the domain Ω, is formulated in terms of the unknown displacement vector $\mathbf{u}$. Based on the principle of virtual work, an incremental form of the equilibrium equation can be written as

$$\left[\int_\Omega \delta\varepsilon^{\mathrm{T}}\,\mathrm{d}\sigma\,\mathrm{d}\Omega - \int_\Omega \delta\mathbf{u}^{\mathrm{T}}\,\mathrm{d}\mathbf{b}\,\mathrm{d}\Omega - \int_\Omega \delta\mathbf{u}^{\mathrm{T}}\mathrm{d}\hat{\mathbf{t}}\,\mathrm{d}\Gamma\right]_1 = 0 \tag{20}$$

Incorporating the effective stress relationship, given as

$$\sigma_1 = (\mathbf{D}_{\mathrm{T}}\varepsilon_1 - \mathbf{m}\bar{P}_1) + \sigma_0 \tag{21}$$

where σ_1 is the total stress, $\mathbf{D}_{\mathrm{T}}$ is the tangential stiffness matrix, ε_1 represents the strain of the medium caused by effective stress only, $\mathbf{m}$ is equal to unity for the normal stress components and zero for the shear stress components, $\bar{P}_1$ is the average pore pressure within sub-domain 1, and σ_{o} is the initial stress, into equation (20) and dividing by $\mathrm{d}t$, the following equation is obtained for three-phase flow:

$$\left[\int_\Gamma \delta\varepsilon^{\mathrm{T}} D_{\mathrm{T}}\frac{\partial\varepsilon}{\partial t}\mathrm{d}\Gamma - \int_\Gamma \delta\varepsilon^{\mathrm{T}}\mathbf{m}\frac{\partial\bar{P}}{\partial t}\mathrm{d}\Omega + \frac{\partial\hat{\mathbf{f}}}{\partial t}\right]_1 = 0 \tag{22}$$

where

$$\mathrm{d}\hat{\mathbf{f}} = -\int_\Omega \delta\mathbf{u}^{\mathrm{T}}\,\mathrm{d}\mathbf{b}\,\mathrm{d}\Omega - \int_\Omega \delta\mathbf{u}^{\mathrm{T}}\mathrm{d}\hat{\mathbf{t}}\,\mathrm{d}\Gamma + \int_\Omega \delta\varepsilon^{\mathrm{T}}\,\mathrm{d}\sigma_{\mathrm{o}}\,\mathrm{d}\Omega \tag{23}$$

Substituting for the derivative term of the average pore pressure, $\mathrm{d}\bar{P}/\mathrm{d}t$, from equation (16) into equation (22) gives the final form of the equilibrium equation as follows:

$$\int_\Omega \delta\varepsilon_1^{\mathrm{T}}\mathbf{D}_{\mathrm{T}}\frac{\partial\varepsilon_1}{\partial t}\mathrm{d}\Omega_1 - \int_{\Omega_1} \delta\varepsilon_1^{\mathrm{T}} S''_{\mathrm{w}1}\mathbf{m}\frac{\partial P_{\mathrm{w}1}}{\partial t}\mathrm{d}\Omega_1 - \int_{\Omega_1} \delta\varepsilon_1^{\mathrm{T}} S''_{\mathrm{o}1}\mathbf{m}\frac{\partial P_{\mathrm{o}1}}{\partial t}\mathrm{d}\Omega_1 - \int_{\Omega_1} \delta\varepsilon_1^{\mathrm{T}} S''_{\mathrm{g}1}\mathbf{m}\frac{\partial P_{\mathrm{g}1}}{\partial t}\mathrm{d}\Omega_1 + \frac{\partial\hat{\mathbf{f}}}{\partial t} = 0 \tag{24}$$

Bearing in mind that the applied loads are carried only by the solid matrix (Assumption 5 Section 2), then the equilibrium equation is developed for the matrix continuum only which is denoted by the subscript 1.

5. DEVELOPMENT OF THE CONTINUITY EQUATIONS

The equations governing the behaviour of three immiscible and compressible fluids flowing in a deforming porous medium can be derived by combining the continuity equation for each phase with Darcy's flow equation and an appropriate equation of state, see for instance Reference 26. The only difference is the inclusion of several factors involving the rock matrix displacements in the calculation of the rate of accumulation for each flowing fluid.

Taking into account all the different inflow/outflow sources for a representative elementary volume (REV), the countinuity equation would be as follows, where a detailed derivation is given

in Reference 31:

$$\nabla^{\mathrm{T}}\left(\frac{-\rho_{i\alpha}\mathbf{K}_{\alpha}}{\mu_{i\alpha}}\nabla P_{i\alpha}\right)+(-1)^{\alpha+1}\rho_{i\alpha}\frac{\bar{\alpha}\mathbf{K}_1}{\mu_{i1}}(P_{i1}-P_{i2})+(\alpha-1)\rho_{\mathrm{stc}}(Q_i)_{\mathrm{stc}}$$
$$+\rho_{i\alpha}\phi_{\alpha}\frac{\partial S_{i\alpha}}{\partial t}+\phi_{\alpha}S_{i\alpha}\frac{\partial\rho_{i\alpha}}{\partial t}+(2-\alpha)\rho_{i\alpha}S_{i\alpha}\mathbf{m}^{\mathrm{T}}\frac{\partial\varepsilon_{\alpha}}{\partial t}=0 \tag{25}$$

In fact, equation (25) exhibits six distinct relationships for $i=\mathrm{o},\mathrm{w},\mathrm{g}$ and $\alpha=1,2$, but may be written for each phase and sub-domain, separately. This may be achieved by substituting the equivalent terms into the equation.

In the case of a three-phase flowing system, the effective fluid permeability, $\mathbf{K}_{i\alpha}$, is the product of the three-phase relative permeability, $k_{ri\alpha}$, with the absolute permeability of the matrix and/or fissured network, $\mathbf{K}_{\alpha}$ i.e.;

$$\mathbf{K}_{i\alpha}=\mathbf{k}_{\alpha}(k_{ri})_{\alpha} \tag{26}$$

where α is a 1 and 2 for the two distinct continua. Also, the density of each phase may be expressed as

$$\rho_{i\alpha}=\frac{(\rho_{i\alpha})_{\mathrm{stc}}}{B_{i\alpha}} \tag{27}$$

where $\rho_{i\alpha}$ and $(\rho_{i\alpha})_{\mathrm{stc}}$ are the densities of each phase within the reservoir and at the standard conditions respectively, and $B_{i\alpha}$ is the formation volume factor of phase i. Furthermore, in order to eleminate the time derivatives of $B_{i\alpha}$ in equation (25), we may introduce the following:

$$\frac{\partial}{\partial t}\left(\frac{1}{B_{i\alpha}}\right)=\frac{\partial}{\partial P_{i\alpha}}\left(\frac{1}{B_{i\alpha}}\right)\frac{\partial P_{i\alpha}}{\partial t}=\left(\frac{1}{B_{i\alpha}}\right)'\frac{\partial P_{i\alpha}}{\partial t} \tag{28}$$

where $(1/B_{i\alpha})'$ is the slope of $B_{i\alpha}$–$P_{i\alpha}$ curve. On substituting equations (26)–(28) into equation (25) and rearranging, the following continuity equations for each fluid phase is finally obtained:

for the oil phase:

$$\nabla^{\mathrm{T}}\left(\frac{-\mathbf{k}_{\alpha}k_{\mathrm{ro}\alpha}}{\mu_{\mathrm{o}\alpha}B_{\mathrm{o}\alpha}}\nabla P_{\mathrm{o}\alpha}\right)+(-1)^{\alpha+1}\frac{\bar{\alpha}\mathbf{k}_1k_{\mathrm{ro}1}}{\mu_{\mathrm{o}1}B_{\mathrm{o}1}}(P_{\mathrm{o}1}-P_{\mathrm{o}2})+(\alpha-1)(Q_{\mathrm{o}})_{\mathrm{stc}}$$
$$+\lambda_{\mathrm{oo}\alpha}\frac{\partial P_{\mathrm{o}\alpha}}{\partial t}+\lambda_{\mathrm{wo}\alpha}\frac{\partial P_{\mathrm{w}\alpha}}{\partial t}+\lambda_{\mathrm{go}\alpha}\frac{\partial P_{\mathrm{g}\alpha}}{\partial t}+(2-\alpha)\frac{S_{\mathrm{o}\alpha}}{B_{\mathrm{o}\alpha}}\mathbf{m}^{\mathrm{T}}\frac{\partial\varepsilon_{\alpha}}{\partial t}=0 \tag{29}$$

where

$$\lambda_{\mathrm{oo}\alpha}=\frac{\phi_{\alpha}}{B_{\mathrm{o}\alpha}}\left(S'_{\mathrm{g}\alpha}-S'_{\mathrm{w}\alpha}+S_{\mathrm{o}\alpha}B_{\mathrm{o}\alpha}\left(\frac{1}{B_{\mathrm{o}\alpha}}\right)'\right) \tag{30}$$

$$\lambda_{\mathrm{wo}\alpha}=\frac{\phi_{\alpha}}{B_{\mathrm{o}\alpha}}S'_{\mathrm{w}\alpha} \tag{31}$$

$$\lambda_{\mathrm{go}\alpha}=-\frac{\phi_{\alpha}}{B_{\mathrm{o}\alpha}}S'_{\mathrm{g}\alpha} \tag{32}$$

similarly, for the water phase:

$$\nabla^{\mathrm{T}}\left(\frac{-\mathbf{k}_{\alpha}k_{\mathrm{rw}\alpha}}{\mu_{\mathrm{w}\alpha}B_{\mathrm{w}\alpha}}\nabla P_{\mathrm{w}\alpha}\right)+(-1)^{\alpha+1}\frac{\bar{\alpha}\mathbf{k}_1 k_{\mathrm{rw}1}}{\mu_{\mathrm{w}1}B_{\mathrm{w}1}}(P_{\mathrm{w}1}-P_{\mathrm{w}2})+(\alpha-1)(Q_{\mathrm{w}})_{\mathrm{stc}}$$
$$+\lambda_{\mathrm{ww}\alpha}\frac{\partial P_{\mathrm{w}\alpha}}{\partial t}+\lambda_{\mathrm{ow}\alpha}\frac{\partial P_{\mathrm{o}\alpha}}{\partial t}+\lambda_{\mathrm{gw}\alpha}\frac{\partial P_{\mathrm{g}\alpha}}{\partial t}+(2-\alpha)\frac{S_{\mathrm{w}\alpha}}{B_{\mathrm{w}\alpha}}\mathbf{m}^{\mathrm{T}}\frac{\partial \varepsilon_{\alpha}}{\partial t}=0 \tag{33}$$

where

$$\lambda_{\mathrm{ww}\alpha}=\frac{\phi_{\alpha}}{B_{\mathrm{w}\alpha}}S'_{\mathrm{w}\alpha}+\phi_{\alpha}S'_{\mathrm{w}\alpha}\left(\frac{1}{B_{\mathrm{w}\alpha}}\right)' \tag{34}$$

$$\lambda_{\mathrm{ow}\alpha}=\frac{\phi_{\alpha}}{B_{\mathrm{w}\alpha}}S'_{\mathrm{w}\alpha} \tag{35}$$

$$\lambda_{\mathrm{gw}\alpha}=0 \tag{36}$$

and finally for gas phase, consisting of two components, namely free gas and the dissolved gas in the oil phase

$$\nabla^{\mathrm{T}}\left(\frac{-\mathbf{k}_{\alpha}k_{\mathrm{rg}\alpha}}{\mu_{\mathrm{g}\alpha}B_{\mathrm{g}\alpha}}\nabla P_{\mathrm{g}\alpha}\right)+\nabla^{\mathrm{T}}\left(R_{\mathrm{so}\alpha}\frac{-\mathbf{k}_1 k_{\mathrm{ro}\alpha}}{\mu_{\mathrm{o}\alpha}B_{\mathrm{o}\alpha}}\nabla P_{\mathrm{o}\alpha}\right)+(-1)^{\alpha+1}\frac{\bar{\alpha}\mathbf{k}_1 k_{\mathrm{rg}1}}{\mu_{\mathrm{g}1}B_{\mathrm{g}1}}(P_{\mathrm{g}1}-P_{\mathrm{g}2})$$
$$+(-1)^{\alpha+1}R_{\mathrm{so}\alpha}\frac{\bar{\alpha}K_1 k_{\mathrm{ro}1}}{\mu_{\mathrm{o}1}B_{\mathrm{o}^1}}(P_{\mathrm{o}1}-P_{\mathrm{o}2})+(\alpha-1)[(Q_{\mathrm{g}})_{\mathrm{stc}}+R_{\mathrm{so}\alpha}(Q_{\mathrm{o}})_{\mathrm{stc}}]$$
$$+\lambda_{\mathrm{gg}\alpha}\frac{\partial P_{\mathrm{g}\alpha}}{\partial t}+\lambda_{\mathrm{og}\alpha}\frac{\partial P_{\mathrm{o}\alpha}}{\partial t}+\lambda_{\mathrm{wg}\alpha}\frac{\partial P_{\mathrm{w}\alpha}}{\partial t}+(2-\alpha)C_{\mathrm{go}\alpha}\mathbf{m}^{\mathrm{T}}\frac{\partial \varepsilon_{\alpha}}{\partial t}=0 \tag{37}$$

where

$$\lambda_{\mathrm{gg}\alpha}=\phi_{\alpha}S_{\mathrm{g}\alpha}\left(\frac{1}{B_{\mathrm{g}\alpha}}\right)'+\phi_{\alpha}\left(\frac{1}{B_{\mathrm{g}\alpha}}-\frac{R_{\mathrm{so}\alpha}}{B_{\mathrm{o}\alpha}}\right)S'_{\mathrm{g}\alpha} \tag{38}$$

$$\lambda_{\mathrm{og}\alpha}=\phi_{\alpha}R_{\mathrm{so}\alpha}S_{\mathrm{o}\alpha}\left(\frac{1}{B_{\mathrm{o}\alpha}}\right)'-\frac{\phi_{\alpha}}{B_{\mathrm{g}\alpha}}S'_{\mathrm{g}\alpha}$$
$$+\frac{R_{\mathrm{so}\alpha}}{B_{\mathrm{o}\alpha}}(\phi_{\alpha}S'_{\mathrm{g}\alpha}-\phi_{\alpha}S'_{\mathrm{w}\alpha})+\phi_{\alpha}\frac{S_{\mathrm{o}\alpha}}{B_{\mathrm{o}\alpha}}R'_{\mathrm{so}\alpha} \tag{39}$$

$$\lambda_{\mathrm{wg}\alpha}=\phi_{\alpha}\frac{R_{\mathrm{so}\alpha}}{B_{\mathrm{o}\alpha}}S'_{\mathrm{w}\alpha} \tag{40}$$

$$C_{\mathrm{go}\alpha}=\frac{S_{\mathrm{g}\alpha}}{B_{\mathrm{g}\alpha}}+R_{\mathrm{so}\alpha}\frac{S'_{\mathrm{o}\alpha}}{B_{\mathrm{o}\alpha}} \tag{41}$$

The term $(Q_i)_{\mathrm{stc}}$ can be either a production or an injection rate depending on the sign give. Here a positive flux value implies a production rate and *vice versa*. Note that the dissolved gas in the oil phase, which appears in equation (37), was assumed to be function of the oil-phase pressure only.

Equations (24), (29), (33) and (37) represent a set of highly non-linear partial differential equations for multi-phase flow coupling with the consolidation behaviour occurring in a deforming fractured oil reservoir. The major non-linearities, i.e. the phase saturation, S_i, relative permeability, k_r, formation volume factor, B_i, gas–oil solution ratio, R_{so}, and viscosity, μ_i, are strongly dependent on the unknowns and therefore should be updated at appropriate time intervals.

6. BOUNDARY CONDITIONS

Generally, the flow boundary condition may be written based on Darcy's equation where the flow rate q_π of the π-phase, which can be either flow in or out of the system, must satisfy the following condition:

$$-\mathbf{n}^T \frac{\mathbf{k} k_{r\pi}}{\mu_\pi} \nabla P_\pi = q_\pi \quad \text{on} \quad \Gamma_\pi \tag{42}$$

where $\pi = o, g, w$ for oil, gas and water, respectively, and $\mathbf{n}^T$ is the unit normal vector. In practice, two different types of flow boundary conditions are usually applied, firstly by prescribing the flow rate:

$$q_\pi = q_{\pi b} \tag{43}$$

or secondly by specifying the value of pressure at the boundary as

$$P_\pi = P_{\pi b} \tag{44}$$

where values $q_{\pi b}$ and $P_{\pi b}$ are the prescribed flow and pressure values, respectively, at the boundary. In the special case of a closed boundary, also known as an 'impermeable' or 'no-flow boundary', the flux should be et equal to zero, i.e. $q_{\pi b} = 0$.

7. INITIAL CONDITIONS

Normally, the initial conditions of a reservoir system can be defined by specifying the initial distribution of fluid pressure within the reservoir and/or its saturation, depending on the unknowns used in the formulation and the updating procedure.Therefore, the initial conditions for a three-dimensional reservoir system can be defined as follows:

$$P^0(x, y, z) = P_i(x, y, z) \tag{45}$$

$$S^0(x, y, z) = S_i(x, y, z) \tag{46}$$

where P^0 is the fluid pressure for node (x, y, z) at time zero, where S^0 is the fluid saturation for node (x, y, z) at time zero, where P_i is the initial fluid pressure in the system and S_i is the initial fluid saturation in the system.

8. FINITE ELEMENT DISCRETIZATION

A Galerkin-based finite element method was applied to the governing equations obtained in the previous section where the displacements, $\mathbf{U}_1$, and fluid pressures, $P_{i\alpha}$, in two overlapping continua, namely the matrix and the fractured network, are the primary unknowns. The

discretization process involves two stages, i.e. the spatial and the temporal discretization. For the spatial discretization, if the unknowns are expressed in terms of their nodal values, the unknown matrix, $\mathbf{X}$ can then be approximated by $\bar{\mathbf{X}}$ as

$$\begin{aligned} \mathbf{U}_1 &\approx \mathbf{N}\bar{\mathbf{U}}_1 \\ \mathbf{P}_1 &\approx \bar{\mathbf{N}}\bar{\mathbf{P}}_1 \\ \mathbf{P}_1 &\approx \bar{\mathbf{N}}\bar{\mathbf{P}}_2 \end{aligned} \tag{47}$$

where overlined parameters represent the nodal values. Applying this approximation to the weak form of equations (24), (29), (33) and (37) would result in the following:

$$\underline{\mathscr{A}}\bar{\mathbf{X}} + \underline{\mathscr{B}}\frac{\mathrm{d}}{\mathrm{d}t}\bar{\mathbf{X}} = \mathbf{R} \tag{48}$$

where;

$$\underline{\mathscr{A}} = \left[\begin{array}{c|ccc|ccc} 0 & 0 & 0 & 0 & 0 & 0 & 0 \\ \hline 0 & \mathbf{W}_{p1}+\mathbf{W}_l & 0 & 0 & -\mathbf{W}_l & 0 & 0 \\ 0 & 0 & \mathbf{H}_{p1}+\mathbf{H}_l & 0 & 0 & -\mathbf{H}_l & 0 \\ 0 & 0 & \mathbf{G}_{kl}+\mathbf{G}_m & \mathbf{G}_{p1}+\mathbf{G}_l & 0 & -\mathbf{G}_m & -\mathbf{G}_l \\ \hline 0 & -\mathbf{W}_l & 0 & 0 & \mathbf{W}_{p2}+\mathbf{W}_l & 0 & 0 \\ 0 & 0 & -\mathbf{H}_l & 0 & 0 & \mathbf{H}_{p2}+\mathbf{H}_l & 0 \\ 0 & 0 & -\mathbf{G}_m & -\mathbf{G}_l & 0 & \mathbf{G}_{k2}+\mathbf{G}_m & \mathbf{G}_{p2}+\mathbf{G}_l \end{array}\right] \tag{49}$$

$$\underline{\mathscr{B}} = \left[\begin{array}{c|ccc|ccc} \mathbf{K}_1 & \mathbf{L}_{w1} & \mathbf{L}_{o1} & \mathbf{L}_{g1} & 0 & 0 & 0 \\ \hline \mathbf{W}_{u1} & \mathbf{W}_{w1} & \mathbf{W}_{o1} & \mathbf{W}_{g1} & 0 & 0 & 0 \\ \mathbf{H}_{u1} & \mathbf{H}_{w1} & \mathbf{H}_{o1} & \mathbf{H}_{g1} & 0 & 0 & 0 \\ \mathbf{G}_{u1} & \mathbf{G}_{w1} & \mathbf{G}_{o1} & \mathbf{G}_{g1} & 0 & 0 & 0 \\ \hline 0 & 0 & 0 & 0 & \mathbf{W}_{w2} & \mathbf{W}_{o2} & \mathbf{W}_{g2} \\ 0 & 0 & 0 & 0 & \mathbf{H}_{w2} & \mathbf{H}_{o2} & \mathbf{H}_{g2} \\ 0 & 0 & 0 & 0 & \mathbf{G}_{w2} & \mathbf{G}_{o2} & \mathbf{G}_{g2} \end{array}\right] \tag{50}$$

$$\bar{\mathbf{X}} = \left[\begin{array}{c} \bar{\mathbf{u}}_1 \\ \hline \bar{\mathbf{P}}_{w1} \\ \bar{\mathbf{P}}_{o1} \\ \bar{\mathbf{P}}_{g1} \\ \hline \bar{\mathbf{P}}_{w2} \\ \bar{\mathbf{P}}_{o2} \\ \bar{\mathbf{P}}_{g2} \end{array}\right] \tag{51}$$

$$\mathbf{R} = \begin{bmatrix} \frac{d\mathbf{f}_1}{dt} \\ \hline 0 \\ 0 \\ 0 \\ \hline \bar{\mathbf{F}}_{w2} \\ \bar{\mathbf{F}}_{o2} \\ \bar{\mathbf{F}}_{g2} \end{bmatrix} \tag{52}$$

The elements of the above matrices are defined in Appendix I.

Also, the time discretisation method may also be regarded as a one-dimensional finite element scheme. Basically, the time domain is divided into a number of elements or *time steps*, and integration is carried out for each step to obtain the variation of the sought variables. The step-by-step integrations may be summed to determine the total change of the parameters. By defining two linear shape functions for the time domain as

$$\mathcal{N}_1 = 1 - \alpha_t, \quad \mathcal{N}_1 = \alpha_t \tag{53}$$

where

$$\alpha_t = \frac{t - t_n}{\Delta t_n} \tag{54}$$

the temporally discretized form of equation (48) will ultimately be as follows:

$$[\underline{\mathscr{B}} + \underline{\mathscr{A}}\Delta t_n \theta]\bar{\mathbf{X}}_{t_n + \Delta t_n} = [\underline{\mathscr{B}} - \underline{\mathscr{A}}\Delta t_n(1 - \theta)]\bar{\mathbf{X}}_{t_n} + \mathbf{R}\Delta t_n \tag{55}$$

which may be written in the expanded form of Appendix I. These equations represent a fully coupled and highly non-linear system, for three-phase flow in a deforming fractured porous media. All the non-linear coefficient matrices are dependent on the values of the sought unknowns and therefore iterative procedures are performed within each time step to obtain the final solution.

9. A THREE-PHASE FLOW EXAMPLE

A three-dimensional, field scale example is presented here to demonstrate the utility of the model and so illustrate the nature of fluid flow in fractured reservoirs. The problem was also used to compare with fractured reservoir models which were part of the sixth SPE comparative solution project for double porosity simulators.[34]

A linear section of reservoir was modelled, Figure 3. Vertically, five layers each having a height of 50 ft (15.2 m) were used. Horizontally, the reservoir was divided into ten 200 ft [61 m] grid blocks. A uniform thickness of 1000 ft [305 m] was used in the y direction. The layer description for the cross-section in given in Table I. Whereas both the shape factors and fracture permeabilities may be determined in terms of matrix block size, the corresponding values given in Reference 26 and presented in Table I were used directly. The oil production rate was calculated as follows:

$$Q_o = I_p \Delta p \tag{56}$$

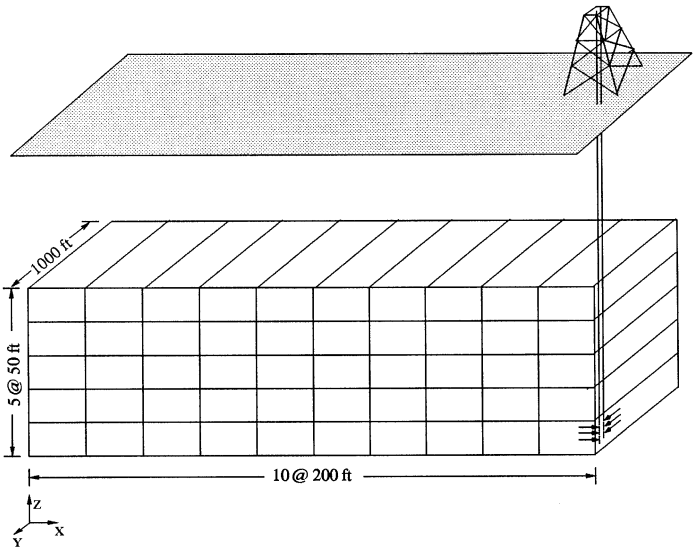

Figure 3. Finite element mesh used for the SPE example (not in scale)

Table I. Basic data for the sixth SPE comparative solution project

Layer	Matrix block size (ft) [m]	Fracture permeability k_2 (md) [m^2]	Shape factor ft^{-2} [m^{-2}]	J (RB-cp)/(D psi) [m^3]
1	25 [7·62]	10 [$9{\cdot}87 \times 10^{-9}$]	0·040 [0·431]	1 [0·0283]
2	25 [7·62]	10 [$9{\cdot}87 \times 10^{-9}$]	0·040 [0·431]	1 [0·0283]
3	5 [1·524]	90 [$8{\cdot}88 \times 10^{-8}$]	1·000 [10·76]	9 [0·2549]
4	10 [3·048]	20 [$1{\cdot}97 \times 10^{-8}$]	0·025 [0·269]	2 [0·0566]
5	10 [3·048]	20 [$1{\cdot}97 \times 10^{-8}$]	0·025 [0·269]	2 [0·0566]

$\mathbf{k}_1$, m [m^2]	1 [$9{\cdot}87 \times 10^{-10}$]
ϕ_1	0·29
ϕ_2	0·01
Initial oil pressure, psi [MPa]	6000 [41·37]
Initial water–oil capillary pressure, psi [Pa]	0·87 [6000]
Initial gas–oil capillary pressure, psi [Pa]	0·02 [500]
Matrix compressibility, vol/vol psi [vol/vol Pa]	$3{\cdot}5 \times 10^{-6}$ [$5{\cdot}075 \times 10^{-10}$]
Z-direction transmissibilities	multiply calculated values by 0·1

where Δp is the well draw-down in psi and I_p is the productivity index, defined as

$$I_p = \frac{k_r J}{B\mu} \tag{57}$$

in which k_r is the oil relative permeability and μ (cp) and B(RB/STB) are the viscosity and formation volume factor of the produced oil, respectively, at well bottom hole pressure (BHP). The coefficient J has dimensions of RB-cp/day-psi, or darcy-ft, and the corresponding values for

Table II. PVT data for the sixth SPE comparative solution project

Pressure (psig)	B_o (RB/STB)	B_g (RB/SCF)	R_s (SCF/STB)	μ_o (cp)	μ_g (cp)	σ (dyne/cm)
1674·0	1·3001	0·00198	367·0	0·529	0·0162	6·0
2031·0	1·3359	0·00162	447·0	0·487	0·0171	4·8
2530·0	1·3891	0·00130	564·0	0·436	0·0184	3·3
2991·0	1·4425	0·00111	679·0	0·397	0·0197	2·2
3553·0	1.5141	0.000959	832·0	0.351	0.0213	1.28
4110·0	1.5938	0·000855	1000·0	0·310	0·0230	0·072
4544·0	1·6630	0·000795	1143·0	0·278	0·0244	0·444
4935·0	1·7315	0·000751	1285·0	0·248	0·0255	0·255
5255·0	1·7953	0·000720	1413·0	0·229	0·0265	0·155
5455·0	1·8540	0·000696	1530·0	0·210	0·0274	0·090
7000·0	2·1978	0·000600	2259·0	0·109	0·0330	0·050

Original bubble point, psig[MPa]	5545[38·23]
Density of stock-tank oil, lbm/cu ft[kg/m^3]	51·14[810·04]
Gas density at standard condition, ibm/cu ft[kg/m^3]	0·058[0·91870]
Water formation volume factor	1·07
Water compressibility, vol/vol psi[vol/vol Pa]	$3{\cdot}5\times10^{-6}[5{\cdot}075\times10^{-10}]$
Water viscosity, cp[Pa s]	$0{\cdot}35[0{\cdot}35\times10^{-3}]$

each layer are given in Table I. The water and gas rates were obtained in terms of the mobility ratio values as follows:

$$Q_w = M_{wo}Q_o \tag{58}$$

$$Q_g = M_{go}Q_o + R_{so}Q_o \tag{59}$$

where M_{wo} and M_{go} are the mobility ratios of water to oil and mobility of gas to oil, respectively, and are calculated as follows:

$$M_{wo} = \frac{k_{rw}/\mu_w B_w}{k_{ro}/\mu_o B_o} \tag{60}$$

$$M_{go} = \frac{k_{rg}/\mu_g B_g}{k_{ro}/\mu_o B_o} \tag{61}$$

The production rates are calculated using data evaluated at the beginning of each time step, i.e. explicit loading is assumed. Depletion runs were carried out to a maximum of 10 yr or whenever production declined to less than 1 STB/day [0·16 stock-tank m^3/day]. The production well has a maximum rate of 500 STB/day [80 stock-tank m^3/day] and was limited by a maximum drawdown of 100 psi[689 KPa]. This well was located at the far right column and perforated only in the bottom layer.

Basic PVT data for the example are given in Table II, Reference 34. Also, Figures 4–7 illustrate the capillary pressure-saturation and saturation-relative permeability curves for water–oil and gas–oil systems, respectively. These curves correspond to the matrix continuum only. For the fracture continuum, as in most double porosity models the capillary pressure was assumed to be zero. However, because of the limitation associated with the formulation, a pseudo-capillary

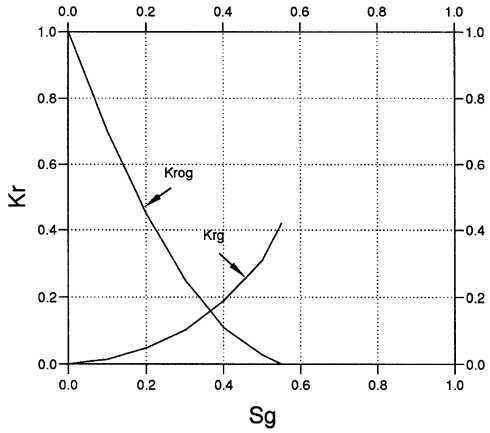

Figure 4. Saturation versus relative permeabilities in the Oil–Gas system for the matrix continuum

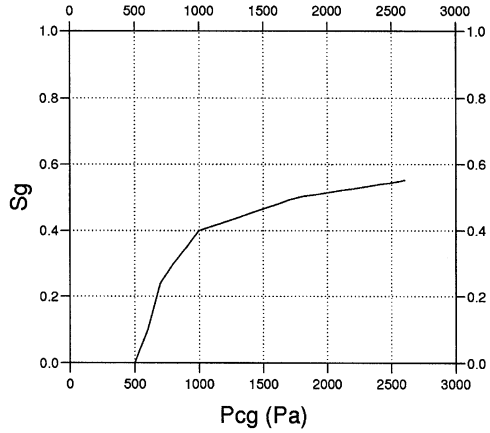

Figure 5. Capillary pressure vs. saturation in the Oil–Gas system for the matrix continuum

pressure curve, having a negligible effect on the depletion behaviour, was assumed. The variation of gas/oil interfacial tension (IFT), σ, with pressure, as given in Table II has also been incorporated into the problem. For this purpose, the gas/oil capillary pressure is directly related to the IFT and therefore the gas/oil capillary pressure should be adjusted according to the ratio of IFT at reservoir pressure divided by the value of the IFT at which the capillary pressure-saturation curve is specified, i.e. bubble point pressure, or in a mathematical form

$$P_{\mathrm{cg}} = \frac{\sigma}{\sigma_I} P_{\mathrm{cg}I} \tag{62}$$

where the term $P_{\mathrm{cg}I}$ corresponds to input capillary pressure values calculated using surface tension σ_I. Adaptive time step incrementing procedure was not applied. Instead, initially 100

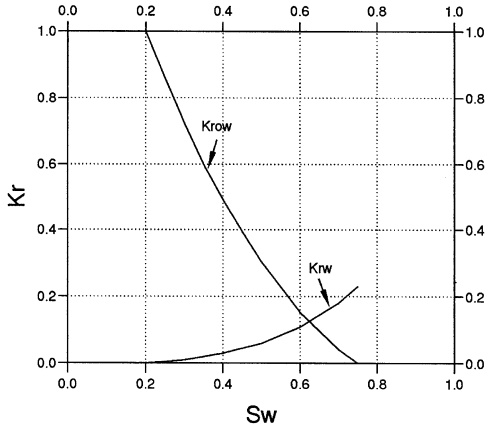

Figure 6. Saturation vs. relative permeabilities in the Oil–Water system for the matrix continuum

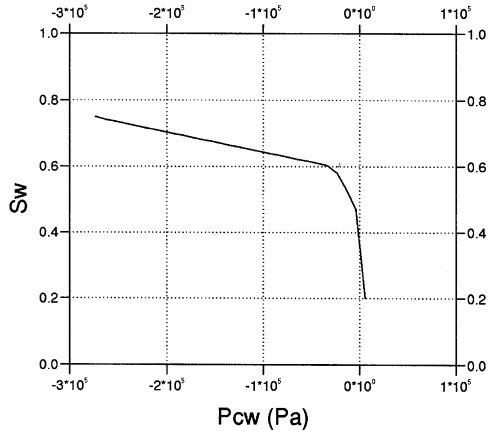

Figure 7. Capillary pressure vs. saturation in the Oil–Water system for the matrix continuum

equally-spaced time step each equal to 0·1 yr were used. Then, in a trial and error manner, the time-step sizes were modified interactively, if a diverging solution occurred. Finally, for the present example the time-step values shown in Table III were found to be satisfactory. The domain was assumed to be sealed and insulated at all boundaries and the displacements, except at the top surface, were assumed to be zero in the directions perpendicular to the faces. Also, the base was assumed to have no movement in all directions.

The Young's modulus of elasticity and Poisson's ratio for the solid porous body were estimated in terms of the compressibility values of the matrix and fractures, and using the following relationship:

$$C = \frac{3(1 - 2v)}{E_s} \tag{63}$$

Table III. Time steps for different time intervals

Time-step size (Year)	Number of time-steps
1.0E-01	80
1.0E-02	65
1.0E-03	77
1.0E-04	15

where C is the compressibility and v and E_s are Young's moduli and Poisson's ratio, respectively.[26]

This reservoir test problem was designed as the sixth SPE comparative solution. The project was to compare various simulators developed using the double porosity model. Ten organizations participated in the solution project. A full description of the models used, can be found in Reference.[34] Generally, all of the models developed were based on the finite difference method and none of them account for the coupling effects between the rock deformation and the fluid flow. Hence, the two salient features of the present study are the use of a fully coupled model and the use of the finite element method as the numerical scheme for the system. The following results were reported by the ten participants:

1. Oil production rate,
2. Gas/Oil ratio, and
3. Pressure values at grid block (5,1,1) for each year.

Also, in order to make a comprehensive comparison, the total number of time-steps and the global iterations for all runs were reported.

Figure 8(a) shows the plot of oil production rate versus elapsed time. With few exceptions, most of the models show similar trends in the reported results. However, the results obtained by the present study, illustrated in Figure 8(b), shows a significantly delayed reduction of the production rate. A negligibly small oscillation of the production rate was observed during the early time steps which could be attributed to the fairly large time intervals in the beginning when the production rate was still high. The oscillation soon damped out after a few time steps. Whereas most of the previous models predict a sharp decline of the production rate after nearly 2–6 yr, the present coupled model predicts a much longer period with a mild slope at the early stages which finally ends after almost 7·5 yr.

The same trend may be observed for the Gas/Oil ratio, GOR, in Figures 9(a) and 9(b). Whilst Figure 9(a) suggests a sharp increase in GOR after a few years due to the decline in reservoir pressure, for the present model, where coupling effects are also considered, this is postponed until the sixth year, see Figure 9(b).

In order to investigate the influence of the reservoir pressure drawdown, the average pressure values in Grid block (5,1,1), obtained by various simulators, are compared in Figures 10(a) and 10(b). The rate of pressure decline in significantly slower when the coupling effect is incorporated, Figure 10(b), whereas all uncoupled models predict a similar trend with a rapidly decreasing pressure, Figure 6.10(a). This confirms the considerable impact of soil deformation on maintaining the initial reservoir pressure for a relatively longer time which can improve long term economical productivity of a reservoir. This effect, which is ignored in conventional uncoupled models, is particularly of great significance when the oil bearing strata are quite deformable.

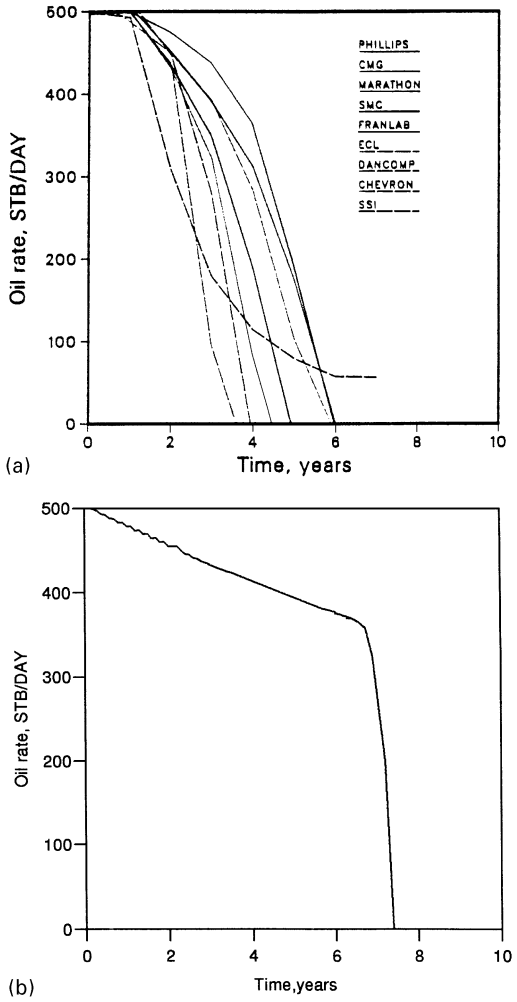

Figure 8. Oil rate vs. time for the SPE example

The next observation deals with a comparison between the number of time steps used by various simulators for the whole time span. As pointed out earlier, unlike previous models, the present simulator does not have the facility of automatic determination of the time-step size, i.e. adaptive time stepping. Rater, the number of time steps and their corresponding sizes are determined by the user based on common engineering sense and therefore is usually a matter of trial and error. As a general rule, in order to ensure the convergence, smaller time steps must be used where a higher production and/or injection rate is expected at a single node. In return, a larger time step size is allowed where production and/or injection rate is relatively small. However, one should bear in mind that the number of time steps must be kept as low as possible to avoid an uneconomic run time. On the other hand, the number of iterations are directly

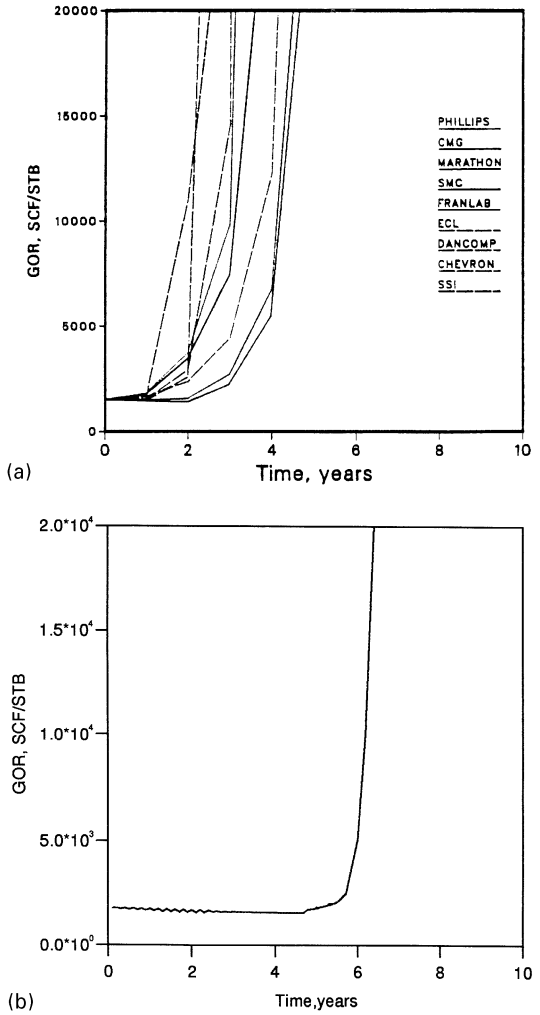

Figure 9. Gas/Oil rate vs. time for the SPE example

proportional to the time-step size: the larger the time-step then the greater number of iterations needed to converge. Since each iteration needs almost the same amount of run time, a balance should be made between the number of iterations and the time step size so that an optimized solution can be obtained. A comparison between the number of time steps used in the present study and those of uncoupled models, indicated in Table IV, implies that the average number of time steps per year is remarkably higher in the present coupled finite element model. This implies that in order to optimize the run time, the efficiency of the program should be further studied and improved.

As pointed out earlier, the impact of coupling between the deformation of the porous media and the fluid flow is particularly important where a highly deformable formation is involved. In

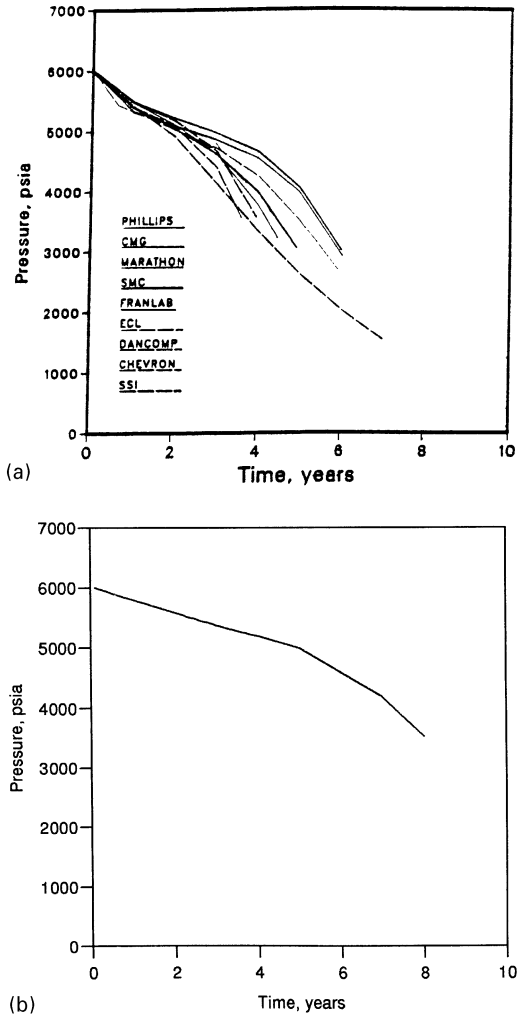

Figure 10. Pressure at Gridblock (5,1,1) vs. time for the SPE example

this case, the soil deformation plays a vital role in maintaining the initial reservoir pressure for a longer time, thus allowing a higher economic productivity for the reservoir. This mechanism, referred to as *compaction drive*, is not predicted by conventional uncoupled models. In order to investigate the significance of the mechanism, three extra runs were also carried out with different moduli of elasticity. The results may be seen in Figures 11–13. As indicated in Figure 11 a longer economic oil production was obtained for the formation having the least modulus value. Also, Figure 12 shows that the sharp increase in Gas/Oil ratio occurs later for the higher moduli values, i.e. for the more deformable formations. The reason may be identified using Figure 13 where the reservoir pressure dissipation is shown to be slower for the lower moduli values.

Table IV. Total number of time steps and global iterations for different simulators

Company (1)	No. of steps (2)	Simulation period (Years) (3)	Ave. no. of step per year (4)	Ave. no. of iter. per step (5)
Philips[a]	48	4·4	10·91	2·42
CMG[b]	63	6·0	10·50	3·80
SMC[c]	53	6·0	8·83	5·00
Marathon[d]	66	5·0	13·20	2·12
Franlab[e]	60	5·0	12·00	3·33
ECL[f]	63	5·9	10·67	4·37
Chevron[g]	36	4·0	9·00	5·40
SSI[h]	75	3·6	20·83	4·11
Dancomp[i]	50	7·0	7·14	5·20
JOE[j]	—	—	—	—
Present Model	237	7·6	31·18	2·41

[a] Philips Petroleum Co.—USA
[b] Computer Modelling Group—Canada
[c] Simulation and Modelling Consultancy Ltd.—England
[d] Marathon Oil Co.—USA
[e] Franlab—France
[f] Exploration Consultants Ltd.—England
[g] Chevron Oil Field Research Co.—USA
[h] Scientific Software-Intercomp—USA
[i] Dancomp A/S—Denmark
[j] Japan Oil Engineering Co.—Japan

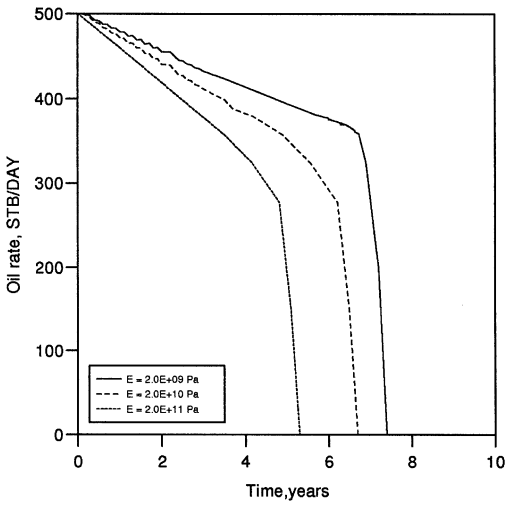

Figure 11. Oil production rate vs. time for three different moduli values

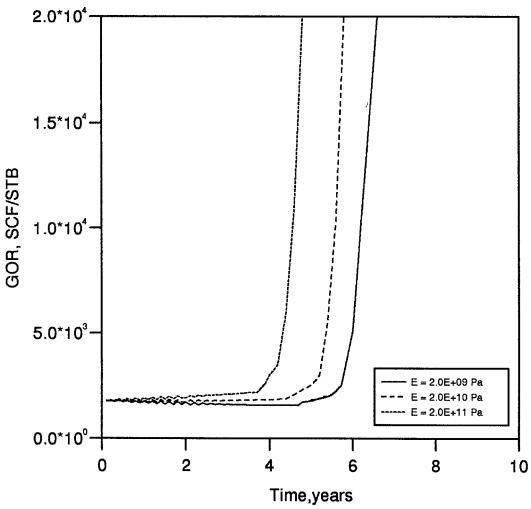

Figure 12. Gas/Oil rate vs. time for three different moduli values

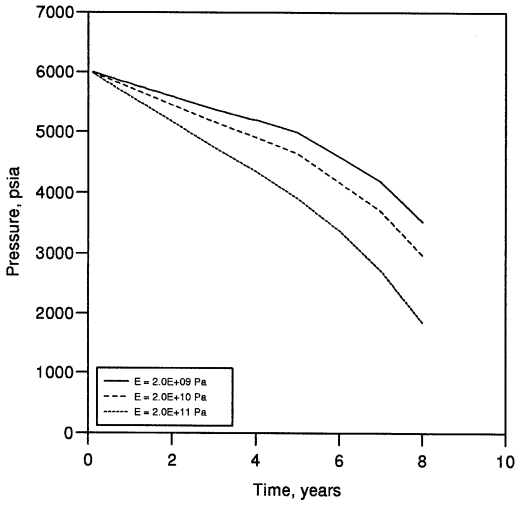

Figure 13. Pressure at Gridblock (5,1,1) vs. time for three different moduli values

10. CONCLUSIONS

A double-porosity coupled reservoir simulator for naturally fractured reservoirs was introduced. For the sake of simplicity, a quasi steady-state transfer function between the fractured and matrix continua was assumed. Any other type of transfer function could similarly be applied. The results obtained by the present model suggest a prolonged economic production period for the reservoir if the impact of coupling between solid deformation and fluid pressure is fully included into the

simulation. The finite element solutions indicate an adverse run time when compared to the other models discretized using the finite difference method. However, it should be noted that the cost is justifiable as the present model included additional independent variables, i.e. reservoir displacements, and therefore a greater number of unknowns are required to converge in order to obtain the final solution for each step. This additional cost, however, cannot undermine the flexibility of the method in modelling complicated geometries as well as boundary conditions The efficiency of the model may be improved by applying adaptive procedures, both for the space and temporal domain, and this is being done as the next stage.

ACKNOWLEDGEMENTS

One of the authors, H. R. Ghafouri, is grateful for the financial support given by the Ministry of Culture and Higher Education of the Islamic Republic of Iran.

NOMENCLATURE

B	formation volume factor,	–
b	body force,	FL^{-3}
d	Fractures interval	L
E	module of elasticity,	FL^{-2}
$\mathbf{K}$	effective fluid permeability,	LT^{-1}
$\mathbf{k}$	absolute permeability,	LT^{-1}
k_r	relative permeability,	–
N	displacement shape function,	–
$\bar{N}$	pressure shape function,	–
N^t	time shape function,	–
P	pore pressure,	FL^{-2}
P_c	capillary pressure,	FL^{-2}
Q	inflow/outflow via sink/source,	L^3T^{-1}
S	saturation,	–
$\hat{t}$	boundary traction,	FL^{-2}
V_1	pore volume in a REV,	L^3
V_2	fissure volume in a REV,	L^3
V	total volume of a REV,	L^3

Greek letters

ϕ_1	matrix porosity,	–
ϕ_2	fracture porosity,	–
ε_v	volumetric strain,	–
$\bar{\alpha}$	fracture shape factor,	L^{-2}
α_0	time-stepping factor,	–
μ	fluid viscosity,	FTL^{-2}
ρ	fluid density,	ML^{-3}
ρ_o	fluid density at a reference point,	ML^{-3}
σ_o	initial stress,	FL^{-2}

σ'	effective stress,	FL^{-2}
σ	total stress,	FL^{-2}
v	Poisson ratio,	–

Super and subscripts

α	denoting matrix (1) and fracture (2) continuum	–
i	denoting fluid phases o, w and g	–
k	iteration level	–
–	nodal values	–
T	transposed matrix	–

APPENDIX I

Various terms of equation (55) may be substituted by their original forms given in equations (49)–(52). This leads to the following expanded form,

$$\left[\begin{array}{c|ccc|ccc} \mathbf{K}_1 & \mathbf{L}_{w1} & \mathbf{L}_{o1} & \mathbf{L}_{g1} & 0 & 0 & 0 \\ \hline \mathbf{W}_{u1} & \mathbf{W}'_1 & \mathbf{W}_{o1} & \mathbf{W}_{g1} & \mathbf{W}' & 0 & 0 \\ \mathbf{H}_{u1} & \mathbf{H}_{w1} & \mathbf{H}'_1 & \mathbf{H}_{g1} & 0 & \mathbf{H}' & 0 \\ \mathbf{G}_{u1} & \mathbf{G}_{w1} & \hat{\mathbf{G}}'_1 & \mathbf{G}'_1 & 0 & \hat{\mathbf{G}}' & \mathbf{G}' \\ \hline 0 & \mathbf{W}' & \mathbf{0} & \mathbf{0} & \mathbf{W}'_2 & \mathbf{W}_{o2} & \mathbf{W}_{g2} \\ 0 & 0 & \mathbf{H}' & 0 & \mathbf{H}_{w2} & \mathbf{H}'_2 & \mathbf{H}_{g2} \\ 0 & 0 & \hat{\mathbf{G}}' & \mathbf{G}' & \mathbf{G}_{w2} & \hat{\mathbf{G}}'_2 & \mathbf{G}'_2 \end{array}\right] \left[\begin{array}{c} \bar{\mathbf{u}}_1 \\ \hline \bar{\mathbf{P}}_{w1} \\ \bar{\mathbf{P}}_{o1} \\ \bar{\mathbf{P}}_{g1} \\ \hline \bar{\mathbf{P}}_{w1} \\ \bar{\mathbf{P}}_{o1} \\ \bar{\mathbf{P}}_{g1} \end{array}\right]_{t_n + \Delta t_n} =$$

(64)

$$\left[\begin{array}{c|ccc|ccc} \mathbf{K}_1 & \mathbf{L}_{w1} & \mathbf{L}_{o1} & \mathbf{L}_{g1} & 0 & 0 & 0 \\ \hline \mathbf{W}_{u1} & \mathbf{W}''_1 & \mathbf{W}_{o1} & \mathbf{W}_{g1} & \mathbf{W}'' & 0 & 0 \\ \mathbf{H}_{u1} & \mathbf{H}_{w1} & \mathbf{H}''_1 & \mathbf{H}_{g1} & 0 & \mathbf{H}'' & 0 \\ \mathbf{G}_{u1} & \mathbf{G}_{w1} & \hat{\mathbf{G}}''_1 & \mathbf{G}''_1 & 0 & \hat{\mathbf{G}}'' & \mathbf{G}'' \\ \hline 0 & \mathbf{W}'' & \mathbf{0} & \mathbf{0} & \mathbf{W}''_2 & \mathbf{W}_{o2} & \mathbf{W}_{g2} \\ 0 & 0 & \mathbf{H}'' & 0 & \mathbf{H}_{w2} & \mathbf{H}''_2 & \mathbf{H}_{g2} \\ 0 & 0 & \hat{\mathbf{G}}'' & \mathbf{G}'' & \mathbf{G}_{w2} & \hat{\mathbf{G}}''_2 & \mathbf{G}''_2 \end{array}\right] \left[\begin{array}{c} \bar{\mathbf{u}}_1 \\ \hline \bar{\mathbf{P}}_{w1} \\ \bar{\mathbf{P}}_{o1} \\ \bar{\mathbf{P}}_{g1} \\ \hline \bar{\mathbf{P}}_{w2} \\ \bar{\mathbf{P}}_{o2} \\ \bar{\mathbf{P}}_{g2} \end{array}\right]_{t_n} + \left[\begin{array}{c} \frac{\mathrm{df}_1}{\mathrm{d}t} \\ \hline 0 \\ 0 \\ 0 \\ \hline \bar{\mathbf{F}}_{w2} \\ \bar{\mathbf{F}}_{o2} \\ \bar{\mathbf{F}}_{g2} \end{array}\right] \Delta t_n$$

where

$$\mathbf{W}'_1 = \mathbf{W}_{w1} + \theta \Delta t_n (\mathbf{W}_{p1} + \mathbf{W}_l) \tag{65}$$

$$\mathbf{H}'_1 = \mathbf{H}_{o1} + \theta \Delta t_n (\mathbf{H}_{p1} + \mathbf{H}_l) \tag{66}$$

$$\hat{\mathbf{G}}'_1 = \mathbf{G}_{o1} + \theta\Delta t_n(\mathbf{G}_{k1} + \mathbf{G}_m) \tag{67}$$

$$\mathbf{G}'_1 = \mathbf{G}_{g1} + \theta\Delta t_n(\mathbf{G}_{p1} + \mathbf{G}_l) \tag{68}$$

$$\mathbf{W}'_2 = \mathbf{W}_{w2} + \theta\Delta t_n(\mathbf{W}_{p2} + \mathbf{W}_l) \tag{69}$$

$$\mathbf{H}'_2 = \mathbf{H}_{o2} + \theta\Delta t_n(\mathbf{H}_{p2} + \mathbf{H}_l) \tag{70}$$

$$\hat{\mathbf{G}}'_2 = \mathbf{G}_{o2} + \theta\Delta t_n(\mathbf{G}_{k2} + \mathbf{G}_m) \tag{71}$$

$$\mathbf{G}'_2 = \mathbf{G}_{g2} + \theta\Delta t_n(\mathbf{G}_{p2} + \mathbf{G}_l) \tag{72}$$

$$\mathbf{W}' = -\theta\Delta t_n\mathbf{W}_l \tag{73}$$

$$\mathbf{H}' = -\theta\Delta t_n\mathbf{H}_l \tag{74}$$

$$\hat{\mathbf{G}}' = -\theta\Delta t_n\mathbf{G}_m \tag{75}$$

$$\mathbf{G}' = -\theta\Delta t_n\mathbf{G}_l \tag{76}$$

$$\mathbf{W}''_1 = \mathbf{W}_{w1} - (1-\theta)\Delta t_n(\mathbf{W}_{p1} + \mathbf{W}_l) \tag{77}$$

$$\mathbf{H}''_1 = \mathbf{H}_{o1} - (1-\theta)\Delta t_n(\mathbf{H}_{p1} + \mathbf{H}_l) \tag{78}$$

$$\hat{\mathbf{G}}''_1 = \mathbf{G}_{o1} - (1-\theta)\Delta t_n(\mathbf{G}_{k1} + \mathbf{G}_m) \tag{79}$$

$$\mathbf{G}''_1 = \mathbf{G}_{g1} - (1-\theta)\Delta t_n(\mathbf{G}_{p1} + \mathbf{G}_l) \tag{80}$$

$$\mathbf{W}''_2 = \mathbf{W}_{w2} - (1-\theta)\Delta t_n(\mathbf{W}_{p2} + \mathbf{W}_l) \tag{81}$$

$$\mathbf{H}''_2 = \mathbf{H}_{o2} - (1-\theta)\Delta t_n(\mathbf{H}_{p2} + \mathbf{H}_l) \tag{82}$$

$$\hat{\mathbf{G}}''_2 = \mathbf{G}_{o2} - (1-\theta)\Delta t_n(\mathbf{G}_{k2} + \mathbf{G}_m) \tag{83}$$

$$\mathbf{G}''_2 = \mathbf{G}_{g2} - (1-\theta)\Delta t_n(\mathbf{G}_{p2} + \mathbf{G}_l) \tag{84}$$

$$\mathbf{W}'' = (1-\theta)\Delta t_n\mathbf{W}_l \tag{85}$$

$$\mathbf{H}'' = (1-\theta)\Delta t_n\mathbf{H}_l \tag{86}$$

$$\hat{\mathbf{G}}'' = (1-\theta)\Delta t_n\mathbf{G}_m \tag{87}$$

$$\mathbf{G}'' = (1-\theta)\Delta t_n\mathbf{G}_l \tag{88}$$

and

$$\mathbf{K}_1 = -\int_{\Omega_1} \mathbf{B}_1^{\mathrm{T}}\mathbf{D}_{\mathrm{T}}\mathbf{B}\,\mathrm{d}\Omega_1 \tag{89}$$

$$\mathbf{L}_{w1} = \int_{\Omega_1} \mathbf{B}^{\mathrm{T}} S''_{w1}\mathbf{m}\bar{\mathbf{N}}\,\mathrm{d}\Omega_1 \tag{90}$$

$$\mathbf{L}_{o1} = \int_{\Omega_1} \mathbf{B}^{\mathrm{T}} S''_{o1}\mathbf{m}\bar{\mathbf{N}}\,\mathrm{d}\Omega_1 \tag{91}$$

$$\mathbf{L}_{g1} = \int_{\Omega_1} \mathbf{B}^{\mathrm{T}} S''_{g1}\mathbf{m}\bar{\mathbf{N}}\,\mathrm{d}\Omega_1 \tag{92}$$

$$\mathrm{d}\mathbf{f}_1 = -\int_{\Omega_1} \mathbf{N}^{\mathrm{T}} \mathrm{d}\mathbf{b}\, \mathrm{d}\Omega_1 - \int_{\Gamma_1} \mathbf{N}^{\mathrm{T}} \mathrm{d}\hat{\mathbf{t}}\, \mathrm{d}\Gamma_1 + \int_{\Omega_1} \mathbf{B}^{\mathrm{T}} \mathrm{d}\sigma_{\mathrm{o}}\, \mathrm{d}\Omega_1 \tag{93}$$

$$\mathbf{H}_{p1} = \int_{\Omega_1} (\nabla \bar{\mathbf{N}})^{\mathrm{T}} \frac{-\mathbf{k}_1 k_{\mathrm{ro}1}}{\mu_{\mathrm{o}1} B_{\mathrm{o}1}} (\nabla \bar{\mathbf{N}})\, \mathrm{d}\Omega_1 \tag{94}$$

$$\mathbf{H}_l = \int_{\Omega_1} \bar{\mathbf{N}} \frac{\bar{\alpha} \mathbf{k}_1 k_{\mathrm{ro}1}}{\mu_{\mathrm{o}1} B_{\mathrm{o}1}} \bar{\mathbf{N}}\, \mathrm{d}\Omega_1 \tag{95}$$

$$\mathbf{H}_{\mathrm{o}1} = \int_{\Omega_1} \bar{\mathbf{N}} \lambda_{\mathrm{oo}1} \bar{\mathbf{N}}\, \mathrm{d}\Omega_1 \tag{96}$$

$$\mathbf{H}_{\mathrm{w}1} = \int_{\Omega_1} \bar{\mathbf{N}} \lambda_{\mathrm{wo}1} \bar{\mathbf{N}}\, \mathrm{d}\Omega_1 \tag{97}$$

$$\mathbf{H}_{\mathrm{g}1} = \int_{\Omega_1} \bar{\mathbf{N}} \lambda_{\mathrm{go}1} \bar{\mathbf{N}}\, \mathrm{d}\Omega_1 \tag{98}$$

$$\mathbf{H}_{u1} = \int_{\Omega_1} \bar{\mathbf{N}} \frac{S_{\mathrm{o}1}}{B_{\mathrm{o}1}} \mathbf{m}^{\mathrm{T}} \mathbf{B}\, \mathrm{d}\Omega_1 \tag{99}$$

$$\mathbf{H}_{p2} = \int_{\Omega_2} (\nabla \bar{\mathbf{N}})^{\mathrm{T}} \frac{-\mathbf{k}_2 k_{\mathrm{ro}2}}{\mu_{\mathrm{o}2} B_{\mathrm{o}2}} (\nabla \bar{\mathbf{N}})\, \mathrm{d}\Omega_2 \tag{100}$$

$$\mathbf{H}_l = \int_{\Omega_2} \bar{\mathbf{N}}^{\mathrm{T}} \frac{\bar{\alpha} \mathbf{k}_1 k_{\mathrm{ro}1}}{\mu_{\mathrm{o}2} B_{\mathrm{o}1}} \bar{\mathbf{N}}\, \mathrm{d}\Omega_2 \tag{101}$$

$$\mathbf{H}_{\mathrm{o}2} = \int_{\Omega_2} \bar{\mathbf{N}}^{\mathrm{T}} \lambda_{\mathrm{oo}2} \bar{\mathbf{N}}\, \mathrm{d}\Omega_2 \tag{102}$$

$$\mathbf{H}_{\mathrm{w}2} = \int_{\Omega_2} \bar{\mathbf{N}}^{\mathrm{T}} \lambda_{\mathrm{wo}2} \bar{\mathbf{N}}\, \mathrm{d}\Omega_2 \tag{103}$$

$$\mathbf{H}_{\mathrm{g}2} = \int_{\Omega_2} \bar{\mathbf{N}}^{\mathrm{T}} \lambda_{\mathrm{go}2} \bar{\mathbf{N}}\, \mathrm{d}\Omega_2 \tag{104}$$

$$\bar{\mathbf{F}}_{\mathrm{o}2} = -\int_{\Omega_2} \bar{\mathbf{N}}^{\mathrm{T}} Q_{\mathrm{o}}\, \mathrm{d}\Omega_2 - \int_{\Gamma_2} \bar{\mathbf{N}} q_{\mathrm{o}}\, \mathrm{d}\Gamma_2 \tag{105}$$

$$\mathbf{W}_{p1} = \int_{\Omega_1} (\nabla \bar{\mathbf{N}})^{\mathrm{T}} \frac{-\mathbf{k}_1 k_{\mathrm{rw}1}}{\mu_{\mathrm{w}1} B_{\mathrm{w}1}} (\nabla \bar{\mathbf{N}})\, \mathrm{d}\Omega_1 \tag{106}$$

$$\mathbf{W}_l = \int_{\Omega_1} \bar{\mathbf{N}} \frac{\bar{\alpha} \mathbf{k}_1 k_{\mathrm{rw}1}}{\mu_{\mathrm{w}1} B_{\mathrm{w}1}} \bar{\mathbf{N}}\, \mathrm{d}\Omega_1 \tag{107}$$

$$\mathbf{W}_{\mathrm{w}1} = \int_{\Omega_1} \bar{\mathbf{N}} \lambda_{\mathrm{ww}1} \bar{\mathbf{N}}\, \mathrm{d}\Omega_1 \tag{108}$$

$$\mathbf{W}_{\mathrm{o}1} = \int_{\Omega_1} \bar{\mathbf{N}} \lambda_{\mathrm{ow}1} \bar{\mathbf{N}}\, \mathrm{d}\Omega_1 \tag{109}$$

$$\mathbf{W}_{g1} = \int_{\Omega_1} \bar{\mathbf{N}}\, \lambda_{gw1}\, \bar{\mathbf{N}}\, d\Omega_1 \tag{110}$$

$$\mathbf{W}_{u1} = \int_{\Omega_1} \bar{\mathbf{N}}\, \frac{S_{w1}}{B_{w1}}\, \mathbf{m}^T \mathbf{B}\, d\Omega_1 \tag{111}$$

$$\mathbf{W}_{p2} = \int_{\Omega_2} (\nabla \bar{\mathbf{N}})^T\, \frac{-\mathbf{k}_2 k_{rw2}}{\mu_{w2} B_{w2}} (\nabla \bar{\mathbf{N}})\, d\Omega_2 \tag{112}$$

$$\mathbf{W}_{l} = \int_{\Omega_2} \bar{\mathbf{N}}^T\, \frac{\bar{\alpha} \mathbf{k}_1 k_{rw1}}{\mu_{w1} B_{w1}}\, \bar{\mathbf{N}}\, d\Omega_2 \tag{113}$$

$$\mathbf{W}_{w2} = \int_{\Omega_2} \bar{\mathbf{N}}^T\, \lambda_{ww2}\, \bar{\mathbf{N}}\, d\Omega_2 \tag{114}$$

$$\mathbf{W}_{o2} = \int_{\Omega_2} \bar{\mathbf{N}}^T\, \lambda_{ow2}\, \bar{\mathbf{N}}\, d\Omega_2 \tag{115}$$

$$\mathbf{W}_{g2} = \int_{\Omega_2} \bar{\mathbf{N}}^T\, \lambda_{gw2}\, \bar{\mathbf{N}}\, d\Omega_2 \tag{116}$$

$$\bar{\mathbf{F}}_{w2} = -\int_{\Omega_2} \bar{\mathbf{N}}^T Q_w\, d\Omega_2 - \int_{\Gamma_2} \bar{\mathbf{N}} q_w\, d\Gamma_2 \tag{117}$$

$$\mathbf{G}_{p1} = \int_{\Omega_1} (\nabla \bar{\mathbf{N}})^T\, \frac{-\mathbf{k}_1 k_{rg1}}{\mu_{g1} B_{g1}} (\nabla \bar{\mathbf{N}})\, d\Omega_1 \tag{118}$$

$$\mathbf{G}_{k1} = \int_{\Omega_1} (\nabla \bar{\mathbf{N}})^T\, R_{so1}\, \frac{-\mathbf{k}_1 k_{ro1}}{\mu_{o1} B_{o1}} (\nabla \bar{\mathbf{N}})\, d\Omega_1 \tag{119}$$

$$\mathbf{G}_{l} = \int_{\Omega_1} \bar{\mathbf{N}}^T\, R_{so1}\, \frac{\bar{\alpha} \mathbf{k}_1 k_{rg1}}{\mu_{g1} B_{g1}}\, \bar{\mathbf{N}}\, d\Omega_1 \tag{120}$$

$$\mathbf{G}_{m} = \int_{\Omega_1} \bar{\mathbf{N}}^T\, R_{so1}\, \frac{\bar{\alpha} \mathbf{k}_1 k_{ro1}}{\mu_{o1} B_{o1}}\, \bar{\mathbf{N}}\, d\Omega_1 \tag{121}$$

$$\mathbf{G}_{g1} = \int_{\Omega_1} \bar{\mathbf{N}}^T\, \lambda_{gg1}\, \bar{\mathbf{N}}\, d\Omega_1 \tag{122}$$

$$\mathbf{G}_{o1} = \int_{\Omega_1} \bar{\mathbf{N}}^T\, \lambda_{og1}\, \bar{\mathbf{N}}\, d\Omega_1 \tag{123}$$

$$\mathbf{G}_{w1} = \int_{\Omega_1} \bar{\mathbf{N}}^T\, \lambda_{wg1}\, \bar{\mathbf{N}}\, d\Omega_1 \tag{124}$$

$$\mathbf{G}_{u1} = \int_{\Omega_1} \bar{\mathbf{N}}^T\, C_{go} \mathbf{m}^T \mathbf{B}\, d\Omega_1 \tag{125}$$

$$\mathbf{G}_{p2} = \int_{\Omega_2} (\nabla \bar{\mathbf{N}})^T\, \frac{-\mathbf{k}_2 k_{rg2}}{\mu_{g2} B_{g2}} (\nabla \bar{\mathbf{N}})\, d\Omega_2 \tag{126}$$

$$\mathbf{G}_{k2} = \int_{\Omega_2} (\nabla \bar{\mathbf{N}})^{\mathrm{T}} R_{\mathrm{so}2} \frac{-\mathbf{k}_2 k_{\mathrm{ro}2}}{\mu_{\mathrm{o}2} B_{\mathrm{o}2}} (\nabla \bar{\mathbf{N}}) \, \mathrm{d}\Omega_2 \tag{127}$$

$$\mathbf{G}_l = \int_{\Omega_2} \bar{\mathbf{N}}^{\mathrm{T}} R_{\mathrm{so}1} \frac{\bar{\alpha} \mathbf{k}_1 k_{\mathrm{rg}1}}{\mu_{\mathrm{g}1} B_{\mathrm{g}1}} \bar{\mathbf{N}} \, \mathrm{d}\Omega_1 \tag{128}$$

$$\mathbf{G}_m = \int_{\Omega_2} \bar{\mathbf{N}}^{\mathrm{T}} R_{\mathrm{so}1} \frac{\bar{\alpha} \mathbf{k}_1 k_{\mathrm{ro}1}}{\mu_{\mathrm{o}1} B_{\mathrm{o}1}} \bar{\mathbf{N}} \, \mathrm{d}\Omega_1 \tag{129}$$

$$\mathbf{G}_{\mathrm{g}2} = \int_{\Omega_2} \bar{\mathbf{N}}^{\mathrm{T}} \lambda_{\mathrm{gg}2} \bar{\mathbf{N}} \, \mathrm{d}\Omega_2 \tag{130}$$

$$\mathbf{G}_{\mathrm{o}2} = \int_{\Omega_2} \bar{\mathbf{N}}^{\mathrm{T}} \lambda_{\mathrm{og}2} \bar{\mathbf{N}} \, \mathrm{d}\Omega_2 \tag{131}$$

$$\mathbf{G}_{\mathrm{w}2} = \int_{\Omega_2} \bar{\mathbf{N}}^{\mathrm{T}} \lambda_{\mathrm{wg}2} \bar{\mathbf{N}} \, \mathrm{d}\Omega_2 \tag{132}$$

$$\bar{\mathbf{F}}_{\mathrm{g}2} = -\int_{\Omega_2} \bar{\mathbf{N}}^{\mathrm{T}} (Q_{\mathrm{g}} + R_{\mathrm{so}2} Q_{\mathrm{o}}) \, \mathrm{d}\Omega_2 + \int_{\Gamma_2} \bar{\mathbf{N}}^{\mathrm{T}} (q_{\mathrm{g}} + R_{\mathrm{so}2} q_{\mathrm{o}}) \, \mathrm{d}\Gamma_2 \tag{133}$$

REFERENCES

1. M. Bai, Q. Ma and J. C. Roegiers, 'Dual porosity behavior of naturally fractured reservoirs', *Int. J. Numer. Anal. Methods Geomech.* **18,** 359–376 (1994).
2. M. Bai, D. Elsworth, J. C. Roegiers, 'Modeling of naturally fractured reservoirs using deformation dependent flow mechanism', *Int. J. Rock Mech. Min. Sci. and Geomech. Abstr.*, **30,** 1185–1191 (1993.
3. E. J. Daniel, 'Fractured reservoirs of middle east', *Bull. Am. Sssoc. Petrol Geol.*, **38**(5)**,** 774–815 (1954).
4. R. H. Dean and L. L. Lo, 'Simulation of naturally fractured reservoirs', *SPERE*, 638–648 (1988).
5. J. O. Duguid, and J. Abela, 'Finite element Galerkin method for flow in fractured porous media, in: O. C. Zienkiewicz, R. H. Gallagher, and C. Taylor eds. *Finite Element Methods in Flow Problems.*' pp. 599–615, UAH Press, Huntsville, Ala. (1974).
6. J. O. Duguid and P. C. Y. Lee, 'Flow in fractured porous media', *Water Resources Research* **13**, 558–556 (1977).
7. L. S.-K. Fung, 'Simulation of block-to-block processes in naturally fractured reserviors', *SPERE*, 477–484 (1991).
8. L. S.-K Fung, 'Numerical simulation of naturally fractured reservoirs', paper SPE 25616, presented at the *SPE Middle East Oil Conf. and Exh.*, Bahrain, 3–6, April 1993.
9. L. S. -K. Fung, and D. A. Collins, 'An evaluation of the improved dual porosity model for the imulation of gravity effects in naturally fractured reservoirs', *J. Can. Petro. Tech.*, **30,** 61–8 (1991).
10. P. S. Huyakorn, B. H. Lester and C. R. Faust, 'Finite element techniques for modelling groundwater flow in fractured aquifers', *Water Resources Research.*, **19,** 1019–1035 (1983).
11. B. L. Litvak, 'Simulation and characterization of naturally fractured reservoirs', *Proc. Reservoir Characterization Conf.*, Dalas, Academic Press, New York City, 1985, 561–83.
12. B. L. Litvak, A. Satter and S. Etebar, 'An analysis of naturally fractured reservoirs performance using a novel fractured reservoir simulator', paper SPE 17615, preented at the *SPE Int. Meet. on Petro. Eng.* Tianjin, 1–4, November, 1988.
13. J. C. S. Long, J. S. Remer, C. R. Wilson and P. A. Witherspoon, 'Porous-media equivalents for networks of discontinuous fractures', *Water Resource Research* **18,** 645–658 (1982).
14. T. N. Narasimhan, 'Multidimensional numerical simulation of fluid flow in fractured porous media', *Water Resource Research* **18,** 1235–47 (1982).
15. A. S. Odeh, 'On steady state behavior of naturally fractured reservoirs', *Trans. AIME*, **234,** 60 (1965).
16. A. Rasmuson and I. Neretnieks, 'Migration of radionuclides in fissured rocks: The influence of micropore diffusion and longitudinal dispersion', *J. Geophys. Res.*, **86,** 3749–58 (1977).
17. R. J. Rossen, 'Simulation of naturally fractured reservoirs with semi-implicit source terms', *Soc. Pet. Eng. J.*, **17,** 201–210 (1977).

18. R. H. Rossen and E. I. Shen, 'Simulation of Gas/Oil drainage and Water/Oil imbibition in naturally fractured reservoirs', *SPERE*, 464–70 (1989).
19. A. M. Saidi, 'Simulation of naturally fractured reservoirs', paper SPE12270 presented at SPE Reservoir Simulation Symposium, San Francisco, 16–18, November 1983.
20. F. Sonier, P. Soulillard and F. T. Blaskovich, 'Numerical simulation of naturally fractured reservoirs', SPERE, 1114—1122 (1988).
21. F. Sonier and R. Eymard, 'A new simulator for naturally fractured reservoirs', paper SPE 16006 presented at *SPE Reservoir Simulation symposium*, San Antonio, 1–4, February 1987.
22. G. I. Barenblatt, I. P. Zheltov and I. N. Kochina, 'Basic concepts in the theory of seepage of homogeneous liquids in fissured rocks', *J. Appl. Math. Mech., USSR* **24,** 126–303 (1960).
23. J. E. Warren and P. J. Root, 'The behavior of naturally fractured reservoirs.', *Soc. Pet. Eng. J. Trans., AIME*, **228,** 245–55 (1963).
24. H. Kazemi, L. Merril, K. Porterfield and P. Zaman, 'Numerical simulation of water–oil flow in naturally fractured reservoirs', *Soc. Pet. Engng J., Trans. AIME*, **261,** 317–26 (1976).
25. H. Kazemi, J. R. Gilman and A. M. Elsharkawy, 'Analytical and numerical solution of oil recovery from fractured reservoirs with empirical transfer functions, *SPERE*, 219–227 (1992).
26. L. K. Thomas, T. N. Dixon and R. G. Pierson, 'Fractured reservoir simulation', *SPERE*, 42–54 (1983).
27. E. C. Aifantis, 'Introducing a multi-porous medium', *Dev. Mech.* **8,** 209–211 (1977).
28. E. C. Aifantis, 'On the response of fissured rocks', *Dev. Mech.* **10,** 249–253 (1979).
29. E. C. Aifantis, 'On the problem of diffusion in solids', *Acta Mechanica.* **37,** 265–296 (1980).
30. N. Khalili-Naghadeh, 'Numerical modelling flow through fractured media', Ph.D. thesis, The Univ. of NSW, Australia, February 1991.
31. H. R. Ghafouri and R. W. Lewis, 'A finite element double porosity model for heterogeneous deformable porous media', *Int. J. Anal. Numer. Methods Geomech.*, **20,** 831–844 (1996).
32. Reiss and H. Louis, 'The reservoir engineering aspects of fractured formation', translated from the French, Edition Technip, Paris, 1980.
33. J. L. Auriault and C. Boutin, 'Deformable porous media with double porosity. Quasi-statics I: Coupling effects', *Transport Porous Media*, **7,** 63–82 (1992).
34. A. Firoozabadi and L. Kent Thomas 'Sixth SPE comparative solution project: Dual-porosity simulators', *J. Petro. Tech.* **42**(6)**,** 710–715 (1990).

